Data-Driven Identification of hyperelastic models by measuring the strain energy density field

Léna Costecalde, Adrien Leygue, Michel Coret, Erwan Verron

Data-Driven Identification of hyperelastic models by measuring the strain energy density field

Lna Costecalde, Adrien Leygue, Michel Coret, Erwan Verron
Nantes Université, École Centrale Nantes, CNRS, GeM, UMR 6183, F-44300, Nantes, France.

October 6, 2023

Abstract

This paper presents a novel method for accurately identifying the large strain elastic response of elastomeric materials. The method combines the Data-Driven Identification (DDI) algorithm with a unique heterogeneous experiment, deviating from the conventional approach of conducting multiple simple experiments. The primary objective of the method is to decouple the experimental process from the fitting technique, relying instead on a single comprehensive experiment to generate an extensive collection of stress and strain energy fields. This collection is then utilized in conjunction with a standard fitting technique to determine the parameters of hyperelastic models. Notably, the approach places significant emphasis on the strain energy density field as a critical factor in model identification, as it encompasses the full material response within a single scalar quantity.

To demonstrate the effectiveness of the proposed approach, a proof-of-concept is provided using synthetic data. The results highlight the efficiency of the method and emphasize the importance of incorporating the strain energy density field for precise model identification, surpassing the reliance on stress data alone. Additionally, the paper introduces several graphical tools to evaluate and analyze the quality of both the generated mechanical fields and the identification results.

The proposed approach offers a more comprehensive representation of the material behavior, and enhances the reliability and prediction capabilities of hyperelastic material models. It holds significant potential for advancing the field of solid mechanics, particularly in accurately characterizing the mechanical responses of elastomeric materials.

1 Introduction

Elastomeric materials are extensively employed in various industries due to their ability to withstand large strains, as well as their applications in shock absorption, sealing, and elasticity. Since the 1940s, researchers have developed numerous models within the framework of hyperelasticity to describe the unique response of these materials to large strains. Recently, He *et al.* conducted a comprehensive review of 85 such models.[1] These models can be categorized as either phenomenological or based on microstructural considerations. Regardless of their specific formulation, they are characterized by a strain energy density function, denoted as W, which can be written in terms of the principal stretch ratios $(\lambda_i)_{i=1,2,3}$ or, in the special case of isotropic materials, of the first two principal strain invariants, I_1 and I_2 (with the third invariant I_3 being equal to 1 due to incompressibility). Practically, these models involve scalar parameters that depend on the specific elastomer under consideration.

The determination of these parameters involves fitting the mechanical response of the models to experimental data, a process commonly known as "identification." Various minimization methods can be employed for this purpose. In the majority of studies, parameter identification is conducted using experimental stress and strain obtained from simple deformation tests, typically including uniaxial tension (UT), planar tension (PT, also referred to as "pure shear"), and equibiaxial tension (ET). The stress-strain curves obtained from these tests are fitted to the selected model, either by considering the whole dataset, or dividing it into four distinct regions to increase accuracy.[2] Although Steinmann et al. have demonstrated that fitting a model solely on a single deformation state, typically UT, leads to poor reliability and prediction capabilities, and that the accuracy heavily relies on the diversity of experimental data used for identification,[3,4] there is a scarcity of comprehensive data sets in the literature. Indeed, two widely recognized

data sets are often considered: those provided by Treloar[5] and Kawabata *et al.*[6] Authors widely used them to validate their models.[7,8]

To address the limitations of identification on multiple experiments, alternative methods have been developed, aiming to incorporate a single comprehensive experiment with a heterogeneous strain field into the identification process. This concept forms the basis of the Finite Element Model Updating (FEMU) technique.[9] FEMU requires the utilization of strain field measurements, such as Digital Image Correlation (DIC). The technique involves a series of finite element computations that aim to replicate the experimental strain field measured during the test. However, FEMU requires the preselection of a hyperelastic model, which is chosen in advance. More generally, this is also typically the case for identification methods based on full-field measurements, such as Virtual Fields Method, Constitutive Equation Gap Method, Equilibrium Gap method or Reciprocity Gap Method.[10,11] More recently, techniques like EUCLID have emerged, expanding upon the FEMU concept by enabling the determination of an appropriate model from a given set of hyperelastic constitutive equations using a single complex experiment.[12]

The present paper proposes a new identification method based on a single complex experiment. More precisely, it has two main objectives:

- Firstly, it aims to explore the benefits of the two aforementioned identification approaches: decoupling the experiments from the fitting technique and relying on a single heterogeneous experiment.

- Secondly, it seeks to conduct the identification process by minimizing the difference to the strain energy density, as opposed to the standard minimization of the difference to stress.

To fulfill these objectives, the Data-Driven Identification (DDI) method, recently proposed by Leygue and co-workers,[13,14] is considered. Roughly speaking, the method consists of computing both stress and strain energy density fields during a complex experiment, i.e. an experiment in which the strain field is heterogeneous, without prescribing the constitutive equation. Once the strain energy field is estimated throughout the experiment, hyperelastic models are fitted.

In the next section, we present the model underlying the synthetic data. We then provide a brief overview of the DDI technique and describe the identification method. Throughout this section, we introduce new graphical

tools that aid in visualizing the strain and strain energy fields, as well as analyzing the results of identification. Following that, Section 3 presents the identification results and compares them to both the results obtained by fitting the stress field and the "exact solution" used to construct the data set.

2 Methods

2.1 Data generation

The data required to apply the proposed technique consists of a series of strain fields measured during the experiment, for example, using DIC (Digital Image Correlation). In this study, we consider the numerical experiment proposed by Dalmat in her PhD thesis.[15]

2.1.1 Sample and loading conditions

The experiment involves the uniaxial tension of a perforated elastomer membrane. Figure 1 illustrates the sample geometry, its mesh, and the boundary conditions for the experiment. The detailed geometry is presented in Fig. 1(a). The corresponding mesh, composed of 3379 nodes and 6108 linear triangular plane stress finite elements, is shown in Figure 1(b).

The loading conditions are also depicted in Fig. 1(b): the lower part of the sample is clamped (orange boundary conditions in the figure), while the top part is subjected to displacement up to 200% stretch in 20 loading steps (green boundary conditions and black arrow in the figure).

2.1.2 Material

The material considered in this study is the classical 8% sulfur-vulcanized Natural latex Rubber, as tested by Treloar,[5] and widely used in numerous papers.[1] It is modeled using a three-term Ogden model:[16]

$$W(\lambda_1, \lambda_2, \lambda_3) = \sum_{i=1}^{3} \frac{\mu_i}{\alpha_i} \left(\lambda_1^{\alpha_i} + \lambda_2^{\alpha_i} + \lambda_3^{\alpha_i} - 3\right), \tag{1}$$

where the six corresponding parameters $(\mu_i, \alpha_i)_{i=1,2,3}$ calculated by Ogden are provided in Table 1. Note that the corresponding shear modulus is[17]

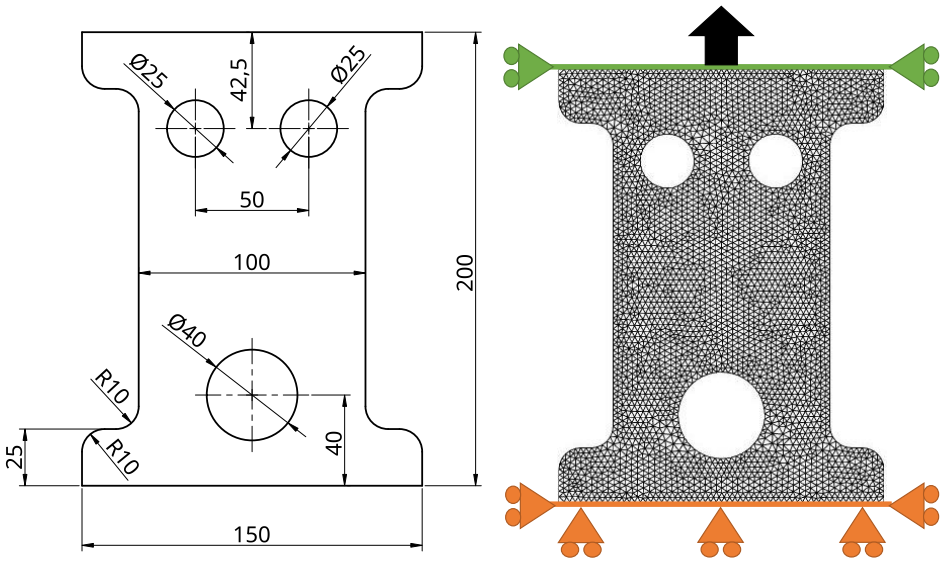

Figure 1: Synthetic experiment: (a) geometry, (b) mesh and boundary conditions.

Parameters	μ_1 (Pa)	μ_2 (Pa)	μ_3 (Pa)	α_1	α_2	α_3
Values	6.18×10^5	1.18×10^3	-9.81×10^3	1.3	5.0	-2.0

Table 1: Material parameters of the three-term Ogden model.

$$\mu = \frac{1}{2} \sum_{i=1}^{3} \mu_i \, \alpha_i \approx 4.14 \times 10^5 \text{ Pa}. \tag{2}$$

2.1.3 From synthetic to experimental data

The previous problem, including the geometry, boundary conditions, and material properties, is solved using the commercial finite element software Abaqus CAE.[18]

From the numerical results, only the kinematic fields (displacement and strain) and the net force that exerts on the top side boundary throughout the test are retained for further analysis. These quantities represent the data that would typically be obtained in a "real" experiment, with the displacement and strain measured using DIC (Digital Image Correlation) and the net force measured using a load cell.

2.1.4 Graphical visualization of kinematical data

To characterize the heterogeneous kinematic field, we employ the Hencky logarithmic strain tensor, also known as the true strain tensor. It is defined as:

$$\boldsymbol{H} = \frac{1}{2} \log \left(\boldsymbol{F}\, \boldsymbol{F}^T \right), \tag{3}$$

where $\boldsymbol{F}$ represents the deformation gradient tensor and $\cdot^T$ denotes transposition. The principal components $\boldsymbol{H}$ can be expressed in terms of stretch ratios: $(H_i = \log \lambda_i)_{i=1,2,3}$.

Inspired by the classical invariants of the Cauchy stress tensor used in plasticity,[19] Criscione *et al.* introduced three interesting invariants of $\boldsymbol{H}$ denoted as K_1, K_2, and K_3.[20] They are defined as follows:

$$K_1 = \mathrm{tr}(\boldsymbol{H}), \quad K_1 \in \Re \tag{4}$$

$$K_2 = \sqrt{\mathrm{dev}(\boldsymbol{H}) : \mathrm{dev}(\boldsymbol{H})}, \quad K_2 > 0 \tag{5}$$

$$K_3 = \frac{3\sqrt{6}}{{K_2}^3} \det(\mathrm{dev}(\boldsymbol{H})), \quad K_3 \in [-1, 1] \tag{6}$$

Here, $\mathrm{dev}(\cdot)$ represents the deviator operator defined as $\cdot - \mathrm{trace}\left((\cdot)/3\right) \boldsymbol{I}$, where $\boldsymbol{I}$ is the identity tensor.

These invariants provide characterization of different aspects of the deformation field. Specifically, they represent the "amount-of-dilatation", the "magnitude-of-distortion", and the "mode-of-distortion", respectively. Since the material is incompressible, the deformation is always isochoric, resulting in $K_1 = 0$. K_2 is a real positive number that increases with the magnitude of strain, while K_3 is a real number that describes the nature of the deformation state. Table 2 presents three particular values of K_3 along with their corresponding deformation states.

K_3	Deformation state
1	Uniaxial tension or equibiaxial compression
0	Planar tension (also known as pure shear)
-1	Uniaxial compression or equibiaxial tension

Table 2: Particular values of K_3 and their corresponding deformation states.

In the following, these invariants are utilized to visualize the strain field obtained from an inhomogeneous experiment. At each time step, for every finite element of the mesh, the Hencky strain tensor $\boldsymbol{H}$ and its invariants K_2 and K_3 (recall $K_1 = 0$) are computed. These values can then plotted as points in the (K_2, K_3)-plane. The shape, density, and size of such scatter plot emphasize the heterogeneity of the strain field within the sample during the experiment.

2.2 Identification method

2.2.1 From kinematic fields to strain energy density field

Data-Driven Identification (DDI) is an algorithm developed by Leygue *et al.*[13] It computes the balanced stress field for a given experiment using a series of strain fields, and without prescribing the constitutive equation. The efficiency of the method is closely related to the variety and the size of the collection of strain fields, also referred to as the "richness" of this collection. It corresponds to the number and distribution of the points in the plot described in Sec. 2.1.4. The technique has been applied to real experiments on elastomers by Dalmat *et al.*[14]

The method's specific details are not reiterated here; interested readers can refer to the aforementioned papers and the references therein. Only a brief overview of the practical steps is provided. The algorithm takes the following inputs:

- Geometry and mesh of the sample, along with the kinematic boundary conditions,
- Measurements of the strain field and the net force throughout the experiment.

Two parameters need to be defined: the ratio r^* between the number of data points, referred to as mechanical states, and the number of stress-strain pairs used to sample the material response, referred to as material states.[13] Additionally, the norm tensor $\mathbb{C}$ is required to determine the distance between mechanical and material states, which needs to be minimized by the algorithm. In this study, the values of r^* ranging from 20 to 75 were investigated, and the best convergence was achieved with $r^* = 44$. This value is used for all subsequent computations. The norm tensor is set as $\mathbb{C} = \beta\mathbb{I}$, where $\mathbb{I}$

represents the fourth-order identity tensor and β is a weighting parameter. To focus solely on the strain fields, β is set to 1×10^6 Pa.

The outputs of the algorithm are:

- The stress fields throughout the experiments,
- The material states that sample the response of the material.

After convergence of the DDI algorithm, the magnitude change between two successive values of the stress tensor is approximately 1×10^{-14} Pa. In the subsequent analysis, only the first output is considered for identifying the constitutive equation.

Considering that the history of the deformation gradient tensor $\boldsymbol{F}(t)$ and the Cauchy stress tensor $\boldsymbol{\sigma}(t)$ is known for the entire mesh, it is possible to compute the strain energy density for each finite element e at each discrete time t_i:

$$W^e_{\mathrm{DDI}_i} = \int_0^{t_i} \boldsymbol{\sigma}^e(t) : \boldsymbol{D}^e(t)\,\mathrm{d}t, \tag{7}$$

where $\boldsymbol{D}$ is the strain rate tensor defined as:

$$\boldsymbol{D} = \mathrm{sym}\left(\dot{\boldsymbol{F}} \cdot \boldsymbol{F}^{-1}\right), \tag{8}$$

with $\mathrm{sym}(\cdot)$ representing the symmetrization operator. Finally, utilizing the previously obtained (K_2, K_3) values from Section 2.1.4, it becomes straightforward to plot the 3D surface of the strain energy density $\left(K^e_{2_i}, K^e_{3_i}, W^e_i\right)$, where the superscript e and subscript i hold the same meaning as in Eq. (7).

2.2.2 Determination of the material parameters

The last step of our Data-Driven Model Identification method involves selecting a hyperelastic model and fitting its parameters to experimental data. Our primary focus will be on fitting the strain energy density, while a secondary fit will be conducted on the stress tensor for comparison purposes.

Let $\boldsymbol{y}$ denote the vector of parameters involved in the model, and $W^e_i(\boldsymbol{y})$ represent the computed strain energy density to be fitted to the measured strain energy $W^e_{\mathrm{DDI}_i}$ data points. The solution $\boldsymbol{y}_{\mathrm{sol}}$ is obtained by minimizing the following objective function:

$$\boldsymbol{y}_{\mathrm{sol}} = \arg\min_{\boldsymbol{y}} \frac{1}{2} \sum_i \sum_e \left(W^e_{\mathrm{DDI}_i} - W^e_i(\boldsymbol{y})\right)^2, \tag{9}$$

where the double summation accounts for all the discrete time steps i and finite elements e.

2.2.3 A graphical tool to discuss the results of identification

To quantitatively analyze the fitting results, we propose a plot illustrating the distribution of relative errors. The plot is constructed as follows:

- The x-axis represents the relative error between the measured strain energy field obtained from the DDI algorithm and the model response, given by $(W_{\mathrm{DDI}} - W)/W_{\mathrm{DDI}}$.
- The y-axis corresponds to the reference field W_{DDI}.
- The distribution of the relative error calculated for every finite elements (e) at every discretized times (i), is plotted on a 100×100 grid. The number of data points within each grid element is counted and divided by the size of the database to obtain the probability of the error. To enhance readability, we consider the logarithm of this probability.

Four examples of such plots, generated using a Gaussian distribution, are shown in Figure 2.

- The top-left graph represents a "perfect fit" scenario, where all errors are zero, and the colorbar depicts the distribution of the experimental data W_{DDI}.
- The top-right graph illustrates a distribution of normally distributed errors centered around zero, i.e. the mean value of W is equal to the one of W_{DDI}, and a standard deviation of 0.1.
- The bottom-left graph shows the distribution of normally distributed relative errors, centered around 0.5, indicating a systematic underestimation of W compared to W_{DDI}.
- The bottom-right graph represents a more realistic scenario, where depending on the measured data, W can either underestimate or overestimate W_{DDI}.

In the next section, we will utilize these tools to analyze the proposed identification method.

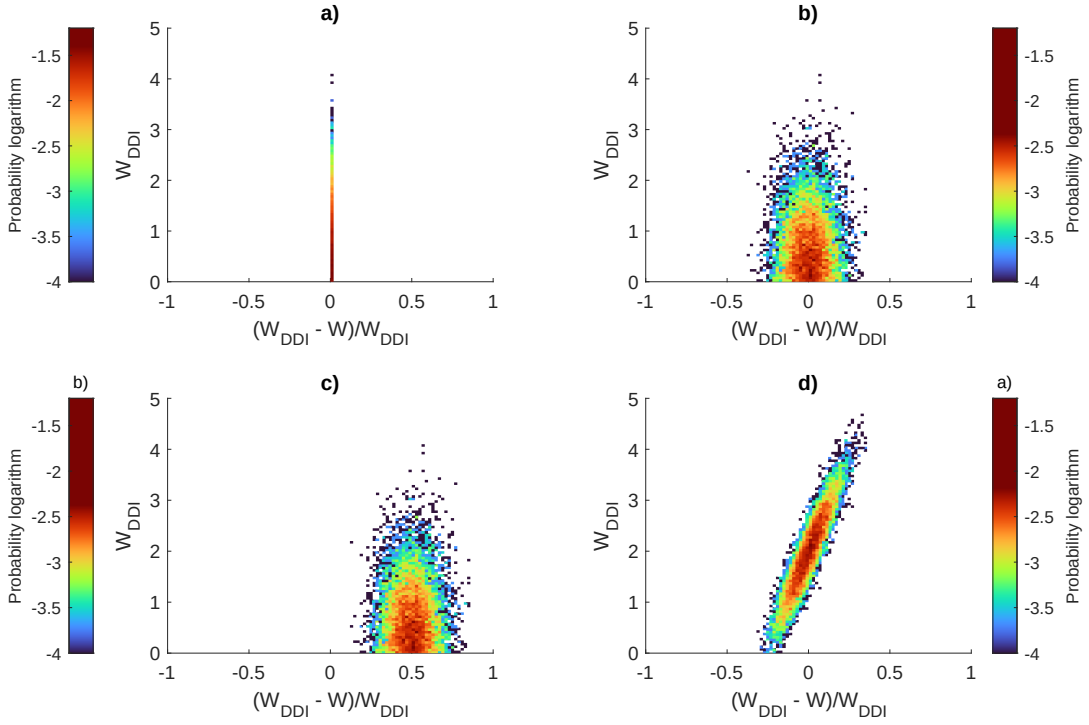

Figure 2: Four examples of error plots.

3 Results and discussion

3.1 Data visualization

First, we display the experimental data using the proposed graphical tools. Figure 3 presents the distribution of strain throughout the entire sample during the experiments. In the figure, the three red dashed lines represent the classical deformation experimental data of Treloar:[5] $K_3 = 1$ for uniaxial tension (UT), $K_3 = 0$ for planar tension (PT), and $K_3 = -1$ for equibiaxial tension (TEQ) (Tab. 2). Despite the majority of experimental points falling within the UT region, it is evident that the entire $(K_2 - K_3)$ plane is explored during the test. Additionally, points are observed in the areas between the simple deformation states. Values of K_3 (horizontal lines) ranging from -1 to 0 describe intermediate deformation states between planar tension and equibiaxial tension, which can be achieved through (non-equibiaxial) biaxial

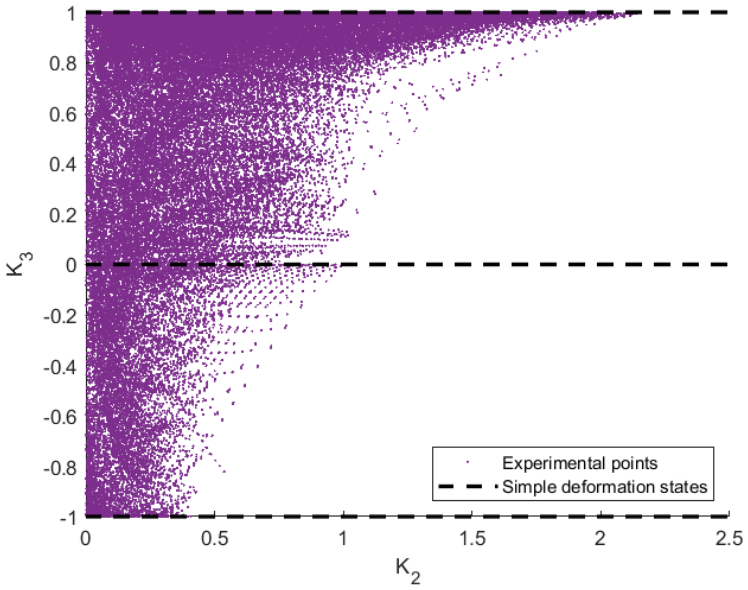

Figure 3: Deformation magnitude and mode in the experiment described in Section 2.1.1. Each black dot represents a specific finite element at a particular time step.

experiments.[6] Values between 0 and 1 describe intermediate deformation states between uniaxial tension and planar tension. As far as we know, there are no technical means to experimentally investigate such states with an homogeneous experiment. The dataset presented here targets mixed modes that are not represented by traditional identification methods using homogeneous deformations fields. Those "blind-spots" of the traditional identification method correspond to real stress-strain scenarios of rubber products in use.

After applying the DDI algorithm, we can visualize the 3D distribution of the strain energy density in relation to the strain state $(K_2 - K_3)$. Figure 4 displays this plot. In this figure, the gray surface represents the analytical solution obtained by computing both the (K_2, K_3) couples (Eqs (3), (5), (6)) and the corresponding strain energy W (Eq. (1)) for a large number of deformation gradient tensors $\boldsymbol{F}$. It is included for visual clarity. The data of Treloar are depicted as black crosses, while our experimental data are represented as purple crosses.

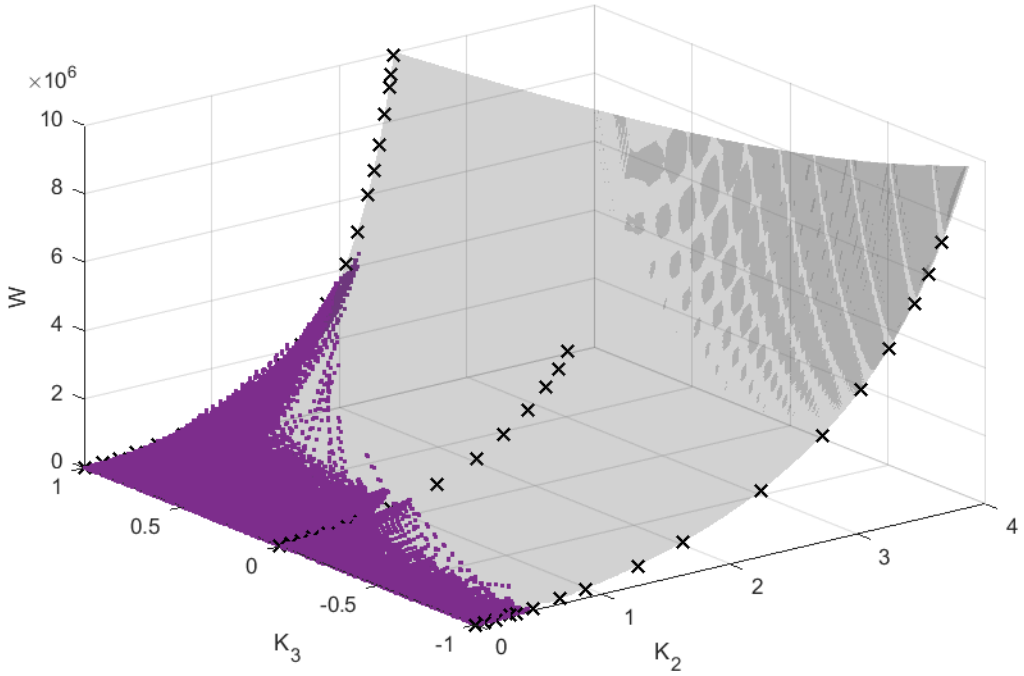

Figure 4: Strain energy response of the sample during the experiment, plotted along Treloar's data.[5]

This figure demonstrates that the DDI technique enables the investigation of a significant range in the material's mechanical response. However, it should be noted that we cannot reach the maximum strain observed in Treloar's experiments, as the maximum global stretch during our experiment is 200%.

3.2 Identification results

Once the data has been established, one or several hyperelastic models can be fitted to this data using Eq. (9). A large number of various hyperelastic models has been derived[1] ; among them we can mention the proposals of Thomas and co-workers.[21,22] To illustrate our approach, we selected here a 3-term Ogden strain energy function, which is the same form than the one used to generate the data. It is well-known that each pair of parameters

(μ_i, α_i) must satisfy $\mu_i\,\alpha_i > 0$ to ensure the polyconvexity of the strain energy function (see, for example the book of Holzapfel[17]). To incorporate this constraint naturally into the identification process, the strain energy density Eq. (1) is expressed in terms of (μ_i, β_i), where $\beta_i = \sqrt{\mu_i\,\alpha_i}$, ensuring that μ_i and α_i have the same sign. The corresponding fitted parameters are presented in Table 3.

Parameters	μ_1 (Pa)	μ_2 (Pa)	μ_3 (Pa)	α_1	α_2	α_3
Results	2.83×10^5	4.66×10^7	-3.15×10^5	1.91	5.85×10^{-4}	-0.84

Table 3: Parameters of a 3-term Ogden model identified with the strain energy density.

First, the shear modulus, calculated using Eq. (2), is approximately 4.16×10^5 Pa. This result indicates that the identification technique successfully preserves the value of the shear modulus.

Secondly, utilizing the graphical tool discussed in Section 2.2.3, the relative error of the identification results is presented in Figure 5. The following

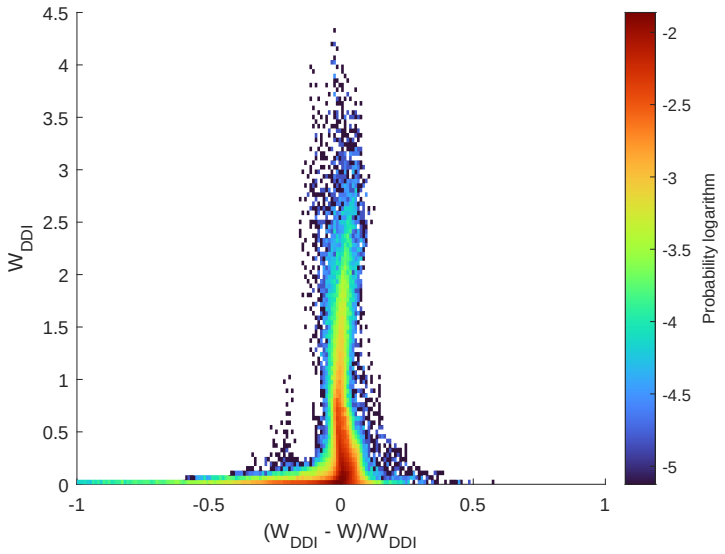

Figure 5: Relative error on the strain energy density.

observations can be made:

- The majority of points align along the vertical $x = 0$ axis, indicating the high quality of the identification.
- The width of the vertical region (approximately between -10% and +10%) represents the scattering of the results, which is relatively small. However, for very small values of the strain energy density, the scattering is more pronounced, primarily due to the error calculation involving division by W_{DDI}.
- The red points (with higher density) correspond to small values of W_{DDI} and are associated with the distribution of measurements shown in Fig. 4 in the vicinity of the $K_2 = 0$ (small strain) axis.

3.3 Why choose the strain energy density for identification?

To discuss the choice of fitting the strain energy density rather than stress data, we modify Eq. (9) by changing the cost function as follow

$$\frac{1}{2}\sum_i \sum_e \left\| \boldsymbol{\sigma}^e_{\mathrm{DDI}_i} - \boldsymbol{\sigma}^e_i(\boldsymbol{y}) \right\|_2^2, \tag{10}$$

$$\text{with } ||\boldsymbol{\sigma}||_2^2 = (\boldsymbol{\sigma} : \boldsymbol{\sigma}) \tag{11}$$

where $\boldsymbol{\sigma}^e_{\mathrm{DDI}_i}$ is the stress tensor in element e at time t_i computed by the DDI algorithm and $\boldsymbol{\sigma}^e_i(\boldsymbol{y})$ is its counterpart calculated by the model.

For a 3-term Ogden model, the fitted parameters are given in Table 4. Both α_1 and α_2 are approximately zero, with magnitudes on the order of

Parameters	μ_1 (Pa)	μ_2 (Pa)	μ_3 (Pa)	α_1	α_2	α_3
Results	4.24×10^5	2.73×10^7	-5.65×10^5	1.74	≈ 0	≈ 0

Table 4: Relative error on the strain energy density for the model identified with the DDI stress field.

10^{-12} and 10^{-11}, respectively. As a result, the model simplifies to a 1-term Ogden model.

Firstly, the shear modulus, calculated using Eq. (2), is approximately 3.69×10^5 Pa. In contrast to the previous case, the current identification process fails to recover the shear modulus of the initial model.

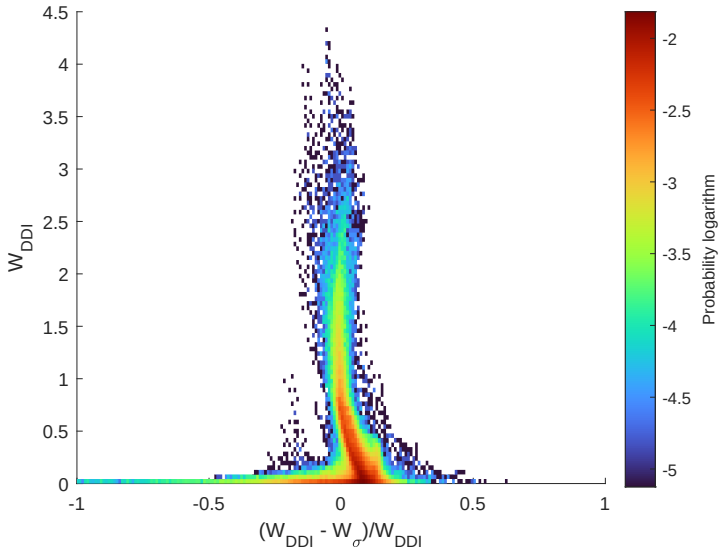

Figure 6: Relative error on the strain energy density for the model identified with experimental stress data.

Second, the error graph is given in Figure 6. The same observations can be made as in the previous case. However, there is some curvature in the scatterplot due to the fact that for small values of W_{DDI}, which correspond to small small, the error deviates from zero. This demonstrates the inadequate prediction of the shear modulus mentioned earlier.

To close this comparison between strain energy and stress identification, the two models respectively defined by Tab. 3 and 4 are compared to the initial one (Tab. 1). The three simple experiments, uniaxial tension, planar tension and equibiaxial tension tests, are compared in Figure 7. The models have been evaluated based on the stretch ratios achieved in Treloar's experiments.[5]

From a global perspective, both models successfully reproduce the material response for the range of stretch ratios used in the identification process. However, there is a discrepancy in the case of uniaxial tension for stretch ratios greater than 4, specifically corresponding to $K_2 > 1.7$. By examining Fig. 3, it is evident that there are very few data points in this region. As a result, these points have minimal impact on the objective function. However, it is important to note that the extrapolated portions of the curves deviate

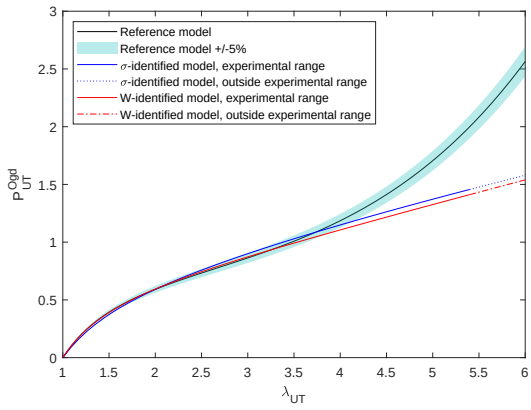

(a) Uniaxial Tension

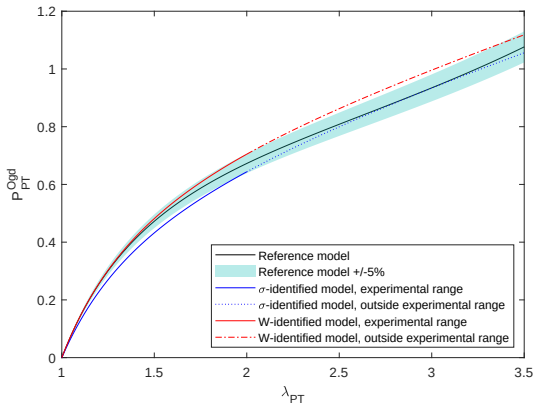

(b) Planar Tension

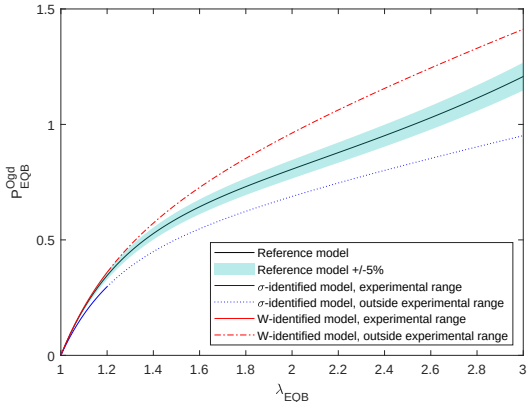

(c) Equibiaxial Tension

Figure 7: Accuracy of the models for the three simple experiments: nominal stress vs. largest stretch ratio for (a) uniaxial tension, (b) planar tension, and (c) equibiaxial tension. The initial model is represented by a black continuous line, and the corresponding stress values are depicted by a sky blue surface with a tolerance of $\pm 5\%$. For each identified model, represented by blue (identified with $\boldsymbol{\sigma}_{\mathrm{DDI}}$) and red (identified with W_{DDI}), the solid line illustrates the model response at stretch ratios achieved by at least one finite element during the heterogeneous test. The dashed and dotted lines are used for extrapolation beyond the tested range.

significantly from the initial model, regardless of the experiment. This observation is a common phenomenon in hyperelasticity. It is widely recognized that accurately predicting the large strain response of elastomers requires relevant data points for model fitting.

Finally, it is worth noting that the small strain predictions in both planar and equibiaxial tension experiments exhibit excellent agreement for the model identified using the strain energy density field. In contrast, the model identified using $\boldsymbol{\sigma}_{\mathrm{DDI}}$ shows relatively poorer agreement in these cases. This discrepancy is primarily attributed to the inaccurate estimation of the shear modulus in the latter model. By considering the strain energy density, the identification process becomes less biased towards uniaxial tension data, which typically provides a large number of data points. This mitigates the potential dominance of a single type of deformation and allows for a more balanced and robust identification of the material behavior.

4 Conclusion

The accurate identification of material mechanical responses remains a persistent challenge in the field of solid mechanics. Numerous methods have been developed to tackle this issue, many of which involve conducting multiple simple experiments. However, the method proposed in this study takes a different approach by combining the Data-Driven Identification (DDI) algorithm with a unique heterogeneous experiment to generate a comprehensive collection of stress and strain energy fields. These fields are then utilized in conjunction with a standard fitting technique for model identification.

The proof-of-concept presented in this paper, using synthetic data, serves to demonstrate the effectiveness of the proposed approach. It not only highlights the efficiency of the method but also underscores the significance of utilizing the strain energy density field for model identification, as opposed to relying classically on stress data. Specifically, the strain energy density field offers the advantage of incorporating different deformation states in a single scalar quantity, allowing for a more comprehensive representation of the material behavior.

While the proof-of-concept demonstrates the efficacy of the approach using synthetic data, further validation and testing on experimental data will be necessary to fully establish its applicability and reliability in real-world scenarios.

References

[1] H. He, Q. Zhang, Y. Zhang, J. Chen, L. Zhang, and F. Li, *Nano Materials Science*, **4**(2) (2022).

[2] L. Han, X. F. Peng, and L. X. Li, *Rubber Chemistry and Technology*, **95**(1), 119 (2022).

[3] P. Steinmann, M. Hossain, and G. Possart, *Archive of Applied Mechanics*, **82**,1183 (2012).

[4] M. Hossain and P. Steinmann, *Journal of the Mechanical Behavior of Materials*, **22**(1-2), 27 (2013).

[5] L. R. G. Treloar, *Rubber Chemistry and Technology*, **17**(4), 813 (1944).

[6] S. Kawabata, M. Matsuda, K. Tei, and H. Kawai, *Macromolecules*, **14**(1), 154 (1981).

[7] M. C. Boyce and E. M. Arruda, *Rubber Chemistry and Technology*, **73**(3), 504 (2000).

[8] G. Marckmann and E. Verron, *Rubber chemistry and technology*, **79**(5), 835 (2006).

[9] P. Ienny, A.-S. Caro-Bretelle, and E. Pagnacco. *European Journal of Computational Mechanics/Revue Européenne de Mécanique Numérique*, **18**(3-4), 353- (2009).

[10] S. Avril, M. Bonnet, A.-S. Bretelle, M. Grédiac, F. Hild, P. Ienny, F. Latourte, D. Lemosse, S. Pagano, E. Pagnacco, and F. Pierron *Experimental Mechanics*, **48**(4), 381 (2008).

[11] B. Pan, *Experimental mechanics*, **51**, 1223 (2011).

[12] M. Flaschel, S. Kumar, and L. De Lorenzis, *Computer Methods in Applied Mechanics and Engineering*, **405**:115867, 2023.

[13] A. Leygue, M. Coret, J. Réthoré, L. Stainier, and Erwan Verron, *Computer Methods in Applied Mechanics and Engineering*, **331**, 184 (2018).

[14] M. Dalémat, M. Coret, A. Leygue, and E. Verron. *Mechanics of Materials*, **136**, 103087 (2019).

[15] M. Dalémat. *Une exprimentation russie pour l'identification de la rponse mcanique sans loi de comportement: Approche data-driven applique aux membranes lastomres*, PhD thesis, École Centrale de Nantes (2019).

[16] R. W. Ogden, *Proceedings of the Royal Society of London. A. Mathematical and Physical Sciences*, **326**(1567), 565 (1972).

[17] G. A. Holzapfel, *Nonlinear Solid Mechanics: a Continuum Approach for Engineering*. John Wiley & Sons, LTD (2000).

[18] Dassault Systemes Simulia Corp. Abaqus cae.

[19] R. M. Brannon, *Shockwave Science and Technology Reference Library, Vol. 2*, Springer Berlin, Heidelberg, Y. Horie editor, 225 (2007).

[20] J. C. Criscione, J. D. Humphrey, A. S. Douglas, and W. C. Hunter, *Journal of the Mechanics and Physics of Solids*, **48**(12), 2445 (2000).

[21] A. N Gent and A. G. Thomas, *Journal of Polymer Science*, **28**(118), 625 (1958).

[22] C. K. L. Davies, D. K. De, and A. G. Thomas, *Rubber Chemistry and Technology*, **67**(4), 716 (1994).